Temperature Induced Volume-Phase Transitions in Surface-Tethered Poly(*N*-isopropylacrylamide) Networks

Ajay Vidyasagar,[†] Jaroslaw Majewski,[‡] and Ryan Toomey*,[†]

Department of Chemical Engineering, 4202 East Fowler Avenue, University of South Florida, Tampa, Florida 33647, and Manuel Lujan Neutron Scattering Center, Los Alamos National Laboratory, Los Alamos, New Mexico 87545

Received June 28, 2007; Revised Manuscript Received November 12, 2007

ABSTRACT: The swelling behavior of a surface-tethered poly(*N*-isopropylacrylamide) (polyNIPAAm) network in D_2O was characterized with neutron reflection and compared to the demixing behavior of linear poly(NIPAAm) in solution. The surface-tethered network was fabricated by cross-linking a 250 Å thick film of a copolymer comprised of NIPAAm and 3 mol % methacroylbenzophenone. As the temperature was varied between 15 and 29 °C, the thickness of the poly(NIPAAm) network in aqueous solution decreased gradually from 1100 to 750 Å. In this regime, the network lay entirely in the single phase region of the phase diagram for linear poly(NIPAAm). At approximately 30 °C, the network entered the two-phase region of the phase diagram and collapsed along the tie line to a thickness of 339 Å. Above 30 °C, the thickness of the network adjusted to the binodal curve of the phase diagram. The agreement between the swelling discontinuity in the surface-tethered network and the two-phase region of uncross-linked poly(NIPAAm) suggests that confinement does not alter the miscibility gap of poly(NIPAAm). With the use of a temperature, T, and polymer volume fraction, ϕ, Flory interaction parameter, $\chi(T,\phi)$, that is tabulated from the demixing data of the linear poly(NIPAAm), the swelling behavior of the surface-tethered network could be modeled using the mean-field Flory−Rehner theory modified for uniaxial swelling.

I. Introduction

Lower critical solution temperature (LCST) polymers experience a sharp volume-phase transition when subjected to small perturbations in external stimuli.[1] For example, it is well-known that poly(*N*-isopropylacrylamide) (poly(NIPAAm)) undergoes a hydrophilic/hydrophobic transition at roughly 32 °C.[2−4] This transition has been attributed to changes in the hydrogen-bonding tendency of water.[5−9] In poly(NIPAAm), it is thought that water molecules form ordered structures around both the hydrophilic amide moieties and the hydrophobic isopropyl groups to maximize favorable hydrogen bonding associations. As temperature is increased, hydrogen bonding interactions grow weaker until the LCST is reached, wherein hydrophobic attractions between isopropyl groups dominate and collapse the polymer structure. While the exact mechanism of this transition remains unknown, tethered LCST polymers are finding success in applications that benefit from reversible modulation of surface properties, including drug delivery,[10,11] separations,[12,13] reversible tissue cultures,[14,15] and chromatography.[16,17]

With respect to the nature of the hydrophilic/hydrophobic transition, aqueous solutions of linear poly(NIPAAm) exhibit a concentration dependent demixing temperature. In particular, Afroze et al. determined that the critical point of poly(NIPAAm) occurs at a temperature of 29.5 °C and a volume fraction, ϕ, of 0.43.[18] As the polymer concentration is reduced toward zero, the demixing temperature approaches 34 °C. To explain this phenomenon, the effective Flory interaction parameter χ can be expanded in powers of ϕ with a minimum of three terms, wherein each term is a function of temperature.[19−21]

A key question concerns the use of a concentration dependent χ parameter derived from solution phase diagrams to describe the behavior of constrained systems, including end-tethered or cross-linked polymers. Baulin and co-workers showed that a self-consistent field theory formulated in terms of a composition dependent χ parameter could lead to a vertical phase separation in poly(NIPAam) brushes.[22] An explicit form of χ was not considered in the study; however, if $\chi(T,\phi)$ could be indeed expanded in powers of ϕ up to the third-order term, bilayer type profiles should be seen in poly(NIPAAm) brushes. Yim and co-workers showed direct experimental evidence of bilayer structures that result from vertical phase separation in poly(NIPAAm) brushes with NR.[23] Mendez and co-workers used the explicit concentration and temperature dependent χ parameter of Afroze et al. to predict compositional profiles of poly(NIPAAm) brushes as a function of temperature.[24] The approach produced results that, at least qualitatively, capture whether or not a brush undergoes a broad or a sharp transition as a function of molecular weight and surface coverage.[25−27]

To permit a simpler comparison between constrained and unconstrained LCST polymers, we report on the swelling of surface-tethered poly(NIPAAm) networks as characterized by neutron reflectivity. Surface tethered-networks produce nearly uniform compositional profiles, thus removing the complication of varying volume fraction profiles found in end-tethered brushes. Harmon and co-workers showed that cross-linked poly(NIPAAm) thin films can undergo significant temperature-induced structural changes with surface plasmon resonance.[28,29] Significantly, the transition temperature appeared to be lower than the cloud temperature observed in linear poly(NIPAAm) solutions.

In this study, surface-tethered networks were prepared from photocross-linkable poly(NIPAAm) copolymers with benzophenone-pendant monomers.[30] Ultraviolet radiation ($\lambda = 350$ nm) triggers the n,π^* transition in the benzophenone moieties leading to a biradicaloid triplet state that abstracts a hydrogen from a neighboring aliphatic C−H group, forming a stable C−C bond.[31]

* Corresponding author.
[†] University of South Florida.
[‡] Los Alamos National Laboratory.

10.1021/ma071438n CCC: $40.75
Published on Web 01/03/2008

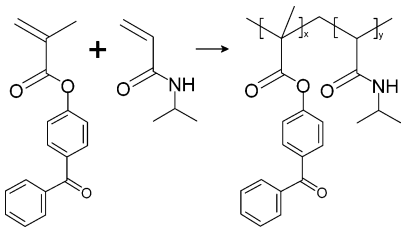

Figure 1. Synthesis of poly(NIPAAm-*co*-MaBP).

Table 1. Physical Characteristics of Poly(NIPAAm-*co*-MaBP)

feed (MaBP)	actual (MaBP)	M_n	M_w/M_n
3.0 mol %	3.0 mol %	42 830 g/mol	4.7

Neutron reflection reveals that the discontinuity in the volume transition of the surface-tethered networks coincides with the miscibility gap of noncross-linked linear poly(NIPAAm). This result signifies that the concentration dependent χ interaction parameter is unaffected by cross-linking and can be used to model volume phase transitions in constrained systems.

II. Experimental Section

Materials. *N*-isopropylacrylamide (NIPAAm), 4-hydroxybenzophenone, methacroyl chloride, triethylamine, acetone, D_2O (99.9 atom %), azobisisobutyronitrile (AIBN), hexanes, diethyl ether, and 3-aminopropyl triethoxysilane were purchased from Sigma. Acetone was distilled from calcium hydride before use, and NIPAAm was recrystallized from hexanes. All other chemicals were used as received.

Monomer Synthesis. Methacroylbenzophenone (MaBP) was synthesized from 4-hydroxybenzophenone and methacroyl chloride in dry acetone at 0 °C. Triethylamine was used as the acid scavenger. The reacted product was run through a column using benzene as the solvent and silica gel as the stationary phase. The monomer was subsequently dried under vacuum. The monomer yield was around 85% MaBP and characterized with an INOVA 400 NMR spectrometer. The spectrum had typical aromatic peaks (multiplet) at 7.2−8.0 and a singlet at 2.1 representing the methyl group characteristic of MaBP.

Copolymer Synthesis. Poly(NIPAAm-*co*-MaBP) was copolymerized with 3 mol % MaBP using 0.1% AIBN as the initiator. The reaction was carried out for 18 h at 65 °C in dioxane under nitrogen. The sample was degassed with nitrogen by freeze and thaw cycles prior to the reaction. After completion, the polymer was precipitated in diethyl ether. The chemical structure is shown in Figure 1, and the physical characteristics are shown in Table 1. The ^1H NMR spectrum is shown in Figure 2. The NH peak shown in the inset and methyl group at 1.0 ppm are characteristic of NIPAAm. The peaks between 7.2 and 8.0 ppm show the aromatic groups of MaBP. The NMR spectrum showed complete incorporation of the MaBP groups. The number average molecular weight was 42 830 g/mol with a polydispersity index of 4.7. Gel permeation chromatography (GPC) was conducted in DMF at 55 °C with a flow rate of 1.0 mL/min (Viscotek GPC Pump; columns: ViscoGel I-series G3000 and G4000 mixed bed columns, molecular weight range 0−60 × 103 and 0−400 × 103 g/mol, respectively). Detection consisted of a Viscotek refractive index detector operating at 660 nm, a Viscotek UV−vis detector operating at 254 nm, and a Viscotek model 270 Series Platform, consisting of a laser light scattering detector (operating at 3 mW, 670 nm with detection angles of 7° and 90°) and a four capillary viscometer. Molecular weights were determined by the triple detection method.

Demixing Temperature of Poly(NIPAAm-*co*-MABP). The sample was placed in a temperature-controlled solution cell. The temperature was ramped at 0.2 °C/min in the temperature range between 15 and 60 °C. The turbidity of the samples was followed during heating by monitoring the scattered light intensity at an angle of approximately 45°. The temperature at which the first deviation of the scattered light intensity from the baseline occurred was taken as the demixing temperature of the corresponding solution.

Preparation of Surface-Tethered Network. Substrates (either quartz or silicon) were cleaned with ozone to remove any organic impurities followed by deposition in a 1% solution of 3-aminopropyltriethoxysilane in acetone. The substrates were heated to 100 °C to drive condensation of the silane groups to the substrate surface. A solution of poly(NIPAM−MaBP) in cyclohexanone was spin cast on the freshly prepared substrate. Cross-linking was accomplished by exposing the film to UV light (365 nm) for 30 min.

Neutron Reflection. Neutron reflection was used to characterize and study the swelling behavior of the poly(NIPAAm-*co*-MaBP) films.[32,33] The neutron reflectivity measurements were carried out on the surface profile analysis reflectometer (SPEAR, Manuel Lujan, Jr. Neutron Scattering Center, Los Alamos National Laboratory, http://www.lansce.lanl.gov/lujan/instruments/SPEAR/). SPEAR is a time-of-flight (TOF) reflectometer employing a polychromatic, pulsed neutron source. The basic principle of neutron reflectometry involves directing a collimated neutron beam toward a flat interface at a low incidence angle, θ, and measuring the ratio of reflected intensity to incident intensity, R, as a function of momentum transfer vector $q_z = 4\pi \sin \theta/\lambda$, where λ is the neutron wavelength. The range of neutron wavelengths used in the experiments was 1−16 Å, determined by the TOF technique. We used two experimental configurations: (i) for measurements in the dry state and against vapors the neutrons were entering quartz or Si substrates from the air (or vapor) side and (ii) an "inverted" geometry with D_2O (solvent) on the bottom and a quartz (or silicon) substrate above the solid−liquid interface. The lower medium has a higher scattering length density than the upper one. Under these conditions, the reflectivity $R = 1$ for q_z below a critical value $q_c = 4\pi(\Delta\text{SLD})^{1/2}$, where ΔSLD is the scattering length density difference between the upper and lower media. Neutron reflectivity data collection typically lasted 1.5−2.5 h. The reflectivity data were reduced using the incident neutron intensity spectrum. On the basis of measured data, a "model" reflectivity profile was generated using Parratt's recursion formalism[34] and compared to the measured reflectivity profile. The model was then adjusted to obtain the best least-squares fit to the data using genetic optimization followed by the Levenberg−Marquardt nonlinear least-squares method.

III. Results and Discussion

We investigated cross-linked poly(NIPAAm-*co*-MaBP) coatings on solid quartz substrates by neutron reflection. All polymers were spin-cast from cyclohexanone followed by heating at 90 °C for 10 min to remove excess solvent. In order to properly constrain the fits of the neutron reflection data, it was important to determine the neutron scattering length density (SLD) of the spin-cast film, which depends on the sum of the bound coherent neutron scattering lengths b_i of the constituent atoms and the molar volume of the polymer layer, defined as the density ρ divided by the molar mass M [32]

$$\text{SLD} = \rho \sum_{i=1}^{n} \frac{b_i}{M} \tag{1}$$

The density of the layer was determined to be 1.2 g/cm^2 as independently measured by X-ray reflection. Hence, the neutron SLD of the spin-cast film was estimated to be 0.96×10^{-6} Å^{-2}.

Figure 3 shows the neutron reflection profile from a 320 Å thick film measured under a dry environment and D_2O vapor at 23 °C. In both cases, the so-called Kiessig fringes persisted over 6 orders of magnitude loss in the reflectivity. In the dry environment, the reflection profile was fit to a single-box model with a scattering length density 0.64×10^{-6} Å^{-2}, which is 33% lower than the expected value of 0.96×10^{-6} Å^{-2}. This discrepancy can be accounted for if bound water is associated

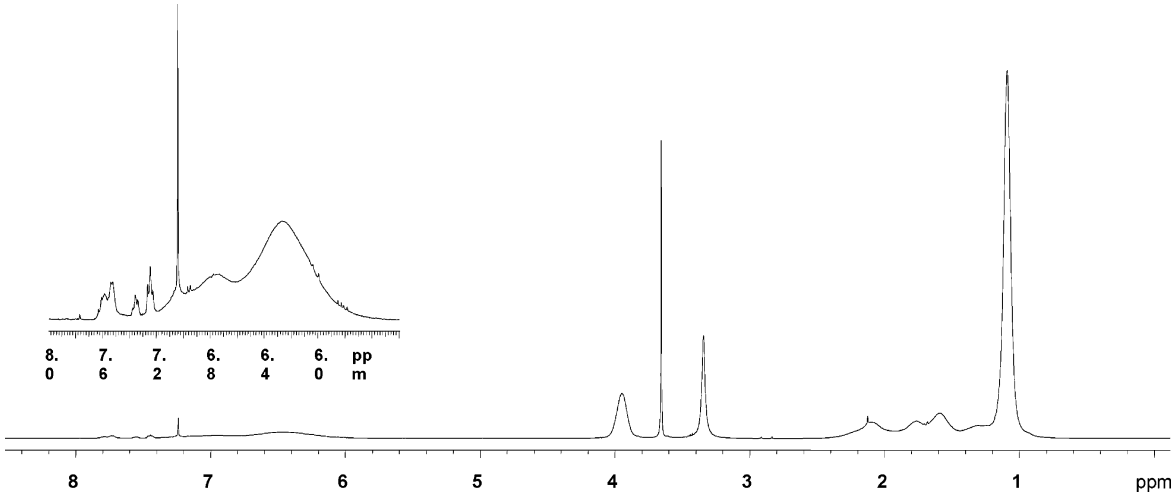

Figure 2. ^{1}H NMR spectrum of poly(NIPAAm-*co*-MaBP(3%)) in $CdCl_3$. The peaks at 1.0 and 4.0 ppm are characteristic of NIPAAm (indicating the CH_3 and CH protons, respectively, associated with the isopropyl group). The peaks between 7.2 and 8.0 ppm are characteristic of MaBP (indicating the nine protons associated with the aromatic groups).

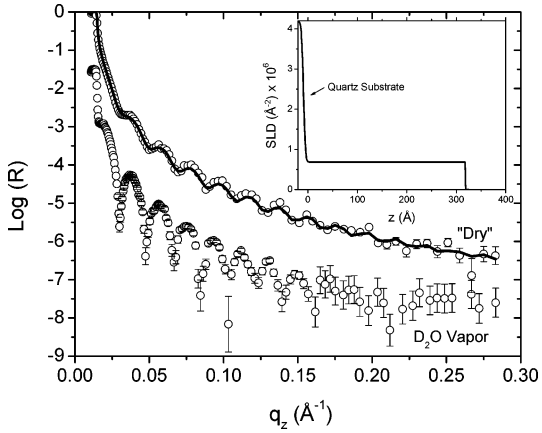

Figure 3. Neutron reflectivity data for surface-tethered poly(NIPAAm-*co*-MaBP) layer in a humidity free "dry" and a D_2O vapor environment at 23 °C. The solid curve drawn through the "dry" data points corresponds to the best fit, which is shown in the inset. The data have been offset vertically for clarity. Error bars for the reflectivity data represent statistical errors in these measurements.

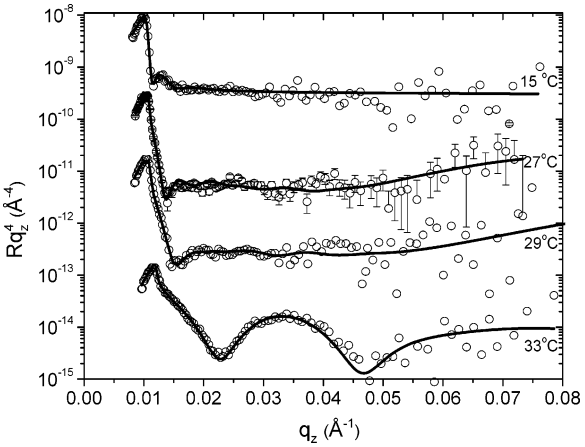

Figure 4. Four examples of the neutron reflectivity data for the surface-tethered poly(NIPAAm-*co*-MaBP) layer exposed to bulk D_2O as a function of temperature. The data and fits (solid lines) have been offset vertically for clarity. The curves through the data correspond to best fits. Error bars for the reflectivity data represent statistical errors in these measurements. The resulting polymer volume fractions, ϕ, at different temperatures are show in Figure 6.

with the poly(NIPAAm) segments. In a two-component system comprising species *i* and *j*, the measured SLD_{layer} is related to sample composition via

$$SLD_{layer} = \phi_i SLD_i + \phi_j SLD_j \quad (2)$$

where $SLD_{i,j}$ is the SLD of each species in the unmixed state, respectively, and $\phi_{i,j}$ is the volume fraction of each species. This relationship assumes that mixing does not affect the molar volumes of either species. Contingent upon an SLD of 0.96×10^{-6} Å^{-2} for dry poly(NIPAAm-*co*-MaBP), the estimated volume fraction of H_2O in the spin-cast layer is 20%. Exposure of the layer to D_2O vapor during the measurement resulted in an increase of the scattering length density to 2.4×10^{-6} Å^{-2}, however the layer thickness increased only 6% to 340 Å. In other words, D_2O replaces H_2O, which enhances contrast but does not significantly alter the thickness. The volume fraction of D_2O in the layer is 25%, similar to H_2O case. On the basis of the contrast variation between H_2O and D_2O, the scattering length density of dry poly(NIPAAm-*co*-MaBP) (without bound water) is estimated to be approximately 0.9×10^{-6} Å^{-2}, which is in agreement with the value calculated using the densities obtained from X-ray reflection.

It needs to be mentioned that rinsing the layer in water for the first time after cross-linking generally resulted in a 5−10% reduction in thickness but no change in the scattering length density. Subsequent rinses did not produce a further loss in material. Additionally, over a 2 month period, measurements from a single sample were reproducible and consistent from run to run, giving us confidence that the films are stable even after repeated solution/dissolution cycles. After each neutron reflectivity experiment of the polymer against bulk liquid, the dry layer was measured and all thicknesses were within 5% of each other. Immediately after a run in D_2O, the SLD of the polymer layer (measured in air) was between approximately 1.0 and 1.5×10^{-6} Å^{-2}, reflecting bound D_2O remaining in the layer. In subsequent measurements, the SLD slowly decayed to 0.6×10^{-6} Å^{-2} as H_2O vapor from the air replaced D_2O.

Figure 4 shows the examples of the neutron reflection profiles and best fits of the poly(NIPAAm-*co*-MABP) layer exposed to bulk D_2O over a temperature range of 15−33 °C. The data are presented as (reflectivity)(q_z^4) to compensate for the q_z^{-4} decay that results from the Fresnel law. The data are shifted on the *y*-axis for clearness. Between 15 and 29 °C, the reflection profile shows a gradual broadening of the first Kiesseg fringe, corre-

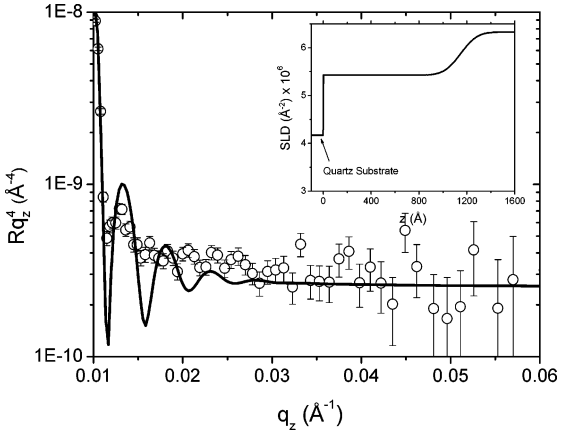

Figure 5. Neutron reflectivity data for surface-tethered poly(NIPAAm-*co*-MaBP) in the D_2O environment at 15 °C. The solid line though the data corresponds to the best fit using a single slab SLD profile. The inset shows the SLD distribution obtained from the best fit.

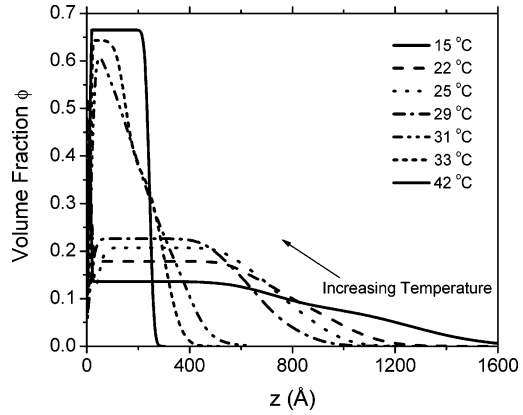

Figure 6. Volume fractions of the poly(NIPAAm-*co*-MaBP) in bulk D_2O as a function of the distance from the substrate and temperature. The data is the outcome of the best fit profiles obtained from fitting neutron reflectivities. The examples of such fits are shown in Figure 4.

sponding to a reduction in the overall thickness of the layer. Between 29 and 33 °C, the spacing between fringes abruptly changes and higher order fringes appear in the reflectivity profile. Above 33 °C the spacing between fringes remain relatively constant with two to three well-defined fringes.

The reflectivity profiles at each temperature were initially modeled using a single slab of constant SLD, with a smeared interface between the layer and solvent. The best fit profiles at low temperatures, however, were inadequate, as shown in Figure 5. A functional form therefore was chosen that consists of three slabs, each of constant SLD, with smeared interfaces between the slabs by error functions. While this simple model was able to produce reasonable fits at all temperatures (Figure 4), we do not exclude the possibility that more complicated models, which describe diffuse interfaces, will provide better fits.[35,36] For instance, there is fine-structure detail that is not captured completely in the three-slab simulations (such as the 27 °C run, Figure 4). However, our attempts to use more sophisticated models, including cubic splines, showed that the fits, while quite sensitive to small changes in interfacial details, did not produce statistical differences in the overall thickness.

The polymer segment profiles that correspond to the best fits in Figure 4 are presented in Figure 6. Each polymer volume fraction profile, $\phi(z)$, was estimated from its scattering length density profile SLD(z) according to eq 2. For every temperature,

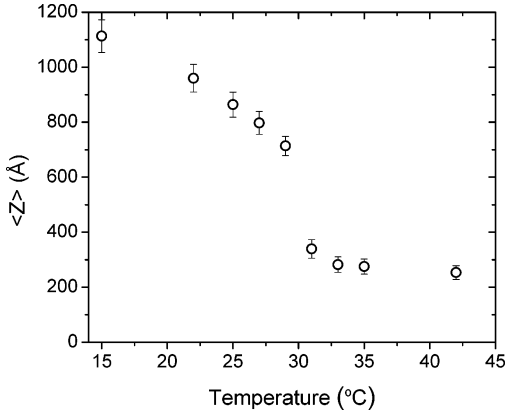

Figure 7. Variation of the average thickness $\langle z \rangle$ of the surface-tethered poly(NIPAAm-*co*-MaBP) network as a function of temperature.

the integral of the volume fraction profile over the extension of the layer was within 5−10% of each other. In other words, although the polymer expands and contracts, its total mass remains constant. The polymer volume fraction profiles show a gradual contraction as temperature is raised from 15 to 29 °C. In this temperature regime, the average thickness decreased from 1100 to 750 Å. The average thickness $\langle z \rangle$ is defined as $(2\int z\phi(z)\,dz)/(\int \phi(z)\,dz)$. Moreover, in every case, a relatively diffuse interface was observed at the D_2O boundary, which was most likely the result of dangling ends that effectively behave as a brush. Between 29 and 31 °C, the average thickness abruptly changes from 714 (±35) Å to 339 (±34) Å. Above 31 °C, the layer thickness continues to contract but is only very weakly dependent on temperature. No discernible difference in layer thickness was observed between 42 °C and 49 °C.

In the high-temperature regime, the volume fraction profiles are nearly uniform with a roughness of approximately 10 Å. Interestingly, there was also a 20−50 Å thick D_2O rich layer next to the substrate, which could be the result of D_2O that cannot escape as the layer collapses. While the nature of this trapped D_2O was not fully investigated in the experiments, repeated temperature cycles showed that the width of the D_2O layer was not consistent from run to run and may be related to the rate of temperature change. The width of the D_2O rich layer, however, did not affect the SLD of the collapsed portion of the poly(NIPAAm-*co*-MaBP) network.

Figure 7 shows the change in the average thickness as a function of temperature. Above 15 °C, the thickness appears to decrease approximately linearly with temperature. At approximately 30 °C, the layer collapses to nearly its thickness as measured in the dry state. This state still contains 30−35% water, which corresponds to two to three D_2O molecules per segment. It is tempting to explain the nature of the collapse based on the experimentally determined phase diagram for linear poly(NIPAAm) solutions. As the demixing temperature of linear poly(NIPAAm) is a strong function of concentration with almost no effect on molecular weight, it is expected that cross-linking will have a minimal effect on the phase behavior.[37−39] Afroze and co-workers fit experimental phase diagrams of linear poly(NIPAAm) with a quadratic form of a compositional dependent χ parameter[18]

$$\chi_{\text{eff}}(T,\phi) = \chi_0(T) + \chi_1(T)\phi + \chi_2(T)\phi^2 \tag{3}$$

where the coefficients depend on temperature via

$$\chi_i(T) = A_i + B_i T \tag{4}$$

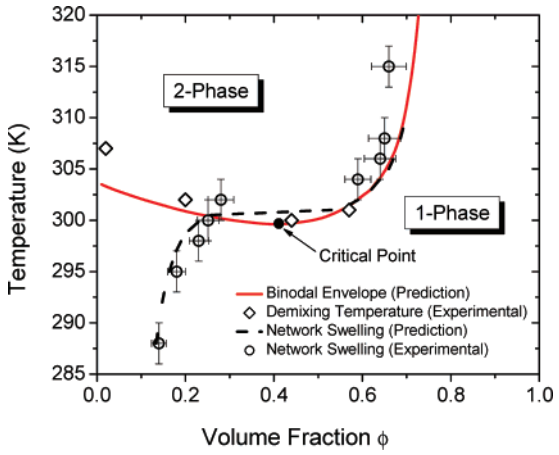

Figure 8. Experimental demixing temperature (◊) of uncross-linked poly(NIPAAm-*co*-MABP) and experimental swelling curve (○) of the surface-tethered poly(NIPAAm-*co*-MABP) network. Also shown are the predicted binodal for linear poly(NIPAAm) at infinite molecular weight and the predicted swelling curve for the surface-tethered network derived from eq 7.

Table 2. Parameters in Equations 2 and 3 for the χ Parameter of Linear Poly(NIPAAm) Solutions Obtained by Afroze et al.[18]

i	A_i	B_i (K^{-1})
0	−12.947	0.04496
1	17.92	−0.0569
2	14.814	−0.0514

The A_i and B_i parameters are given in Table 2. Using these parameters, the phase diagram is drawn in Figure 8 showing the binodal boundaries. The binodal curve envelopes the two-phase region or the miscibility gap of poly(NIPAAm). Superimposed on the binodal are the experimentally determined demixing temperatures for poly(NIPAAm-*co*-MaBP), as determined by turbidity measurements. The degree of agreement between the demixing behavior of poly(NIPAAm-*co*-MaBP) and the data of Afroze et al. is not surprising for two reasons: (1) The demixing temperature of poly(NIPAAm) has been shown to be relatively independent of molecular weight and (2) the 3% mole content of MaBP in poly(NIPAAm-*co*-MABP) is not significant enough to perturb phase behavior.

The extent of dilution in uncross-linked systems can be arbitrarily controlled; therefore, any part of the phase diagram can be accessed. Cross-linked systems, on the other hand, constrain the extent of dilution. The open circles on the phase diagram represent the polymer volume fraction of the surface-tethered poly(NIPAAm-*co*-MABP) network as a function of temperature. The polymer volume fractions were determined from the flat regions of segmental profiles given in Figure 6, where edge effects do not play a role. In the temperature regime of 15−29 °C, the network lay entirely in the single phase region of the phase diagram for linear poly(NIPAAm). In the single phase region, the degree of dilution is determined by a competition between the osmotic pressure arising from contacts between segments (favoring dilution) and the entropic penalty of chain stretching (opposing dilution). As temperature is increased, the osmotic pressure decreases and the network contracts. At approximately 30 °C, the swelling curve of the network enters the two-phase region of the phase diagram. Here, a three-phase equilibrium is established between a pure solvent phase, a swollen polymer-poor network phase, and a contracted polymer-rich network phase. This resultant three-phase equilibrium must be invariant in a binary system at fixed pressure, and, hence, a concentration jump must occur in the network at the temperature of interference. Above 30 °C, the network follows the polymer-rich coexistence curve of the phase diagram.

Using the χ_{eff} parameter from eqs 3−4, we can attempt to model the equilibrium swelling of the network within the Flory−Rehner framework.[40,41] The free energy density $\Delta G_{network}$ of a perfect *phantom* network prepared with ν_e effective mesh chains per unit volume is

$$\frac{\Delta G_{network}}{kT} = (1-\phi)\ln(1-\phi) + \phi(1-\phi)\chi_{eff}(\phi,T) + \frac{1}{2}\nu_e[\alpha_x^2 + \alpha_y^2 + \alpha_z^2 - 3 + \ln(\alpha_x\alpha_y\alpha_z)] \quad (5)$$

k is the Boltzmann constant and α_i is the linear deformation of network in the i direction. The first two terms account for the mixing of polymer and solvent and the last term accounts for elastic deformation of the network. For one-dimensional swelling,[30,42] $\alpha_x = \alpha_y = 1$ *and* $\alpha_z = \phi_0/\phi$, *which equals the swollen ratio of the network relative to its preparation state and* ϕ_0 *is the polymer volume fraction in the relaxed state at the time of cross-linking.*

The equilibrium swelling state is found by setting the chemical potential of the solvent μ_s in the network

$$\frac{\mu_s}{kT} = \frac{\partial(\Delta G_{network}/\phi)}{\partial(1/\phi)} \quad (6)$$

equal to its bulk value (which in a pure solvent is zero):

$$\frac{\mu_s}{kT} = 0 = \ln(1-\phi_e) + \phi_e + \left[\chi_{eff} + \frac{\partial\chi_{eff}}{\partial\phi}\phi_e\right]\phi_e^2 + \frac{\phi_0}{N_{eff}}\left[\left(\frac{\phi_e}{\phi_0}\right)^{-1} - \frac{\phi_e}{2\phi_0}\right] \quad (7)$$

where N_{eff} is the effective degree of polymerization between cross-links. The only adjustable parameter in the model is N_{eff}, which when set to 100 produces good agreement between the model and the experimental data. The model is represented by the dashed black line on the phase diagram in Figure 8. While the agreement between model and experiment is encouraging, there are still a few caveats. Application of eqs 3 and 4 at temperatures and compositions beyond the range of the experimental data used to fit the parameters A_i and B_i may not be appropriate. Second, the deformation term in eq 5 assumes that the network is prepared from equilibrium Gaussian coils, which may not be an appropriate assumption in thin, spin-cast films. Finally, the value of N_{eff} is not explicitly known, but is a fit parameter.

Nonetheless, despite these shortcomings, the swelling discontinuity in the surface-attached network coincides with the two-phase region of uncross-linked poly(NIPAAm). In other words, the demixing temperature of the network is the same as the equivalent uncross-linked system implying that chain conformation does not significantly affect the transition temperature. Consequently, the two-phase region serves as a potential guide for anticipating volume-phase transitions in networks. For instance, a lower cross-link density is expected to result in a slightly higher demixing temperature and larger discontinuity in swelling (on account that the network would enter a wider region of the two-phase region). On the other hand, if the network is constrained to the region below the critical condition, the network is expected to show a smooth volume transition. Experiments are currently underway to test these

hypotheses as well as the adequacy of using the χ_{eff} parameter in eqs 3 and 4 for different states of cross-linking.

IV. Conclusions

Surface-tethered poly(NIPAAm-*co*-MaBP) networks in D_2O were characterized with neutron reflection and compared to the demixing behavior of linear poly(NIPAAm) in solution. The change in thickness of the surface-tethered network as the temperature was increased from 15 to 49 °C was considerable, permitting comparison of the network to the phase behavior of uncross-linked poly(NIPAAm). Interestingly, both the swelling of the network and the demixing behavior of the linear poly(NIPAAm) could be explained with the same concentration-dependent Flory χ parameter. While these experiments do not shed light on the molecular interpretation of the composition dependence, they do point to the idea that constraints on linear chains do not alter this dependence. Consequently, the binodal envelope for the two-phase region in solutions of linear poly(NIPAAm) serves as a potential guide for understanding volume-phase transitions in networks and other confined geometries.

Acknowledgment. This work was supported by the Camille and Henry Dreyfus Foundation, NSF Grant DMR-0645574, USF College of Engineering, and Los Alamos National Laboratory under DOE Contract W7405-ENG-36, the DOE Office of Basic Energy Science. We thank Dr. Brent Summerlin at Southern Methodist University for providing the GPC analysis of the polymer.

References and Notes

(1) Shibayama, M.; Tanaka, T. *Adv. Polym. Sci.* **1993**, *109*, 1−62.
(2) Heskins, M.; Guillet, J. E.; James, E. *J. Macromol. Sci., Chem.* **1968**, *2* (8), 1441−55.
(3) Tanaka, T. *Polymer* **1979**, *20* (11), 1404.
(4) Schild, H. G. *Prog. Polym. Sci.* **1992**, *17* (2), 163−249.
(5) Maeda, Y.; Nakamura, T.; Ikeda, I. *Macromolecules* **2001**, *34* (5), 1391.
(6) Meersman, F.; Wang, J.; Wu, Y. Q.; Heremans, K. *Macromolecules* **2005**, *38* (21), 8923.
(7) Cheng, H.; Shen, L.; Wu, C. *Macromolecules* **2006**, *39* (6), 2325.
(8) Katsumoto, Y.; Tanaka, T.; Sato, H.; Ozaki, Y. *J. Phys. Chem. A* **2002**, *106* (14), 3429−3435.
(9) Okada, Y.; Tanaka, F. *Macromolecules* **2005**, *38* (10), 4465.
(10) Hoffman, A. S. *MRS Bull.* **1991**, *16* (9), 42−46.
(11) Stayton, P. S.; Shimoboji, T.; Long, C.; Chilkoti, A.; Chen, G. H.; Harris, J. M.; Hoffman, A. S. *Nature* **1995**, *378* (6556), 472−474.
(12) Cunliffe, D.; Alarcon, C. D.; Peters, V.; Smith, J. R.; Alexander, C. *Langmuir* **2003**, *19* (7), 2888−2899.
(13) Huber, D. L.; Manginell, R. P.; Samara, M. A.; Kim, B. I.; Bunker, B. C. *Science* **2003**, *301* (5631), 352−354.
(14) Kushida, A.; Yamato, M.; Konno, C.; Kikuchi, A.; Sakurai, Y.; Okano, T. *J. Biomed. Mater. Res.* **1999**, *45* (4), 355.
(15) Kwon, O. H.; Kikuchi, A.; Yamato, M.; Sakurai, Y.; Okano, T. *J. Biomed. Mater. Res.* **2000**, *50* (1), 82.
(16) Kikuchi, A.; Okano, T. *Prog. Polym. Sci.* **2002**, *27* (6), 1165.
(17) Kobayashi, J.; Kikuchi, A.; Sakai, K.; Okano, T. *Anal. Chem.* **2001**, *73* (9), 2027.
(18) Afroze, F.; Nies, E.; Berghmans, H. *J. Mol. Struct.* **2000**, *554* (1), 55.
(19) Moerkerke, R.; Koningsveld, R.; Berghmans, H.; Dusek, K.; Solc, K. *Macromolecules* **1995**, *28* (4), 1103.
(20) Solc, K.; Dusek, K.; Koningsveld, R.; Berghmans, H. *Collect. Czech. Chem. Commun.* **1995**, *60* (10), 1661.
(21) Erman, B.; Flory, P. J. *Macromolecules* **1986**, *19* (9), 2342−2353.
(22) Baulin, V. A.; Zhulina, E. B.; Halperin, A. *J. Chem. Phys.* **2003**, *119* (20), 10977−10988.
(23) Yim, H.; Kent, M. S.; Satija, S.; Mendez, S.; Balamurugan, S. S.; Balamurugan, S.; Lopez, G. P. *Phys. Rev. E* **2005**, 72, (5).
(24) Mendez, S.; Curro, J. G.; McCoy, J. D.; Lopez, G. P. *Macromolecules* **2005**, *38* (1), 174−181.
(25) Balamurugan, S.; Mendez, S.; Balamurugan, S. S.; O'Brien, M. J.; Lopez, G. P. *Langmuir* **2003**, *19* (7), 2545−2549.
(26) Yim, H.; Kent, M. S.; Mendez, S.; Lopez, G. P.; Satija, S.; Seo, Y. *Macromolecules* **2006**, *39* (9), 3420.
(27) Yim, H.; Kent, M. S.; Satija, S.; Mendez, S.; Balamurugan, S. S.; Balamurugan, S.; Lopez, C. P. *J. Polym. Sci., Part B: Polym. Phys.* **2004**, *42* (17), 3302−3310.
(28) Harmon, M. E.; Kuckling, D.; Frank, C. W. *Macromolecules* **2003**, *36* (1), 162−172.
(29) Harmon, M. E.; Jakob, T. A. M.; Knoll, W.; Frank, C. W. *Macromolecules* **2002**, *35* (15), 5999.
(30) Toomey, R.; Freidank, D.; Ruhe, J. *Macromolecules* **2004**, *37* (3), 882−887.
(31) Prucker, O.; Naumann, C. A.; Ruhe, J.; Knoll, W.; Frank, C. W. *J. Am. Chem. Soc.* **1999**, *121* (38), 8766.
(32) Russell, T. P. *Annu. Rev. Mater. Sci.* **1991**, *21*, 249−268.
(33) Lu, J. R.; Thomas, R. K. *J. Chem. Soc., Faraday Trans.* **1998**, *94* (8), 995−1018.
(34) Parratt, L. G. *Phys. Rev.* **1954**, *95*, 359−369.
(35) Yim, H.; Kent, M. S.; Matheson, A.; Stevens, M. J.; Ivkov, R.; Satija, S.; Majewski, J.; Smith, G. S. *Macromolecules* **2002**, *35* (26), 9737−9747.
(36) Yim, H.; Kent, M.; Matheson, A.; Ivkov, R.; Satija, S.; Majewski, J.; Smith, G. S. *Macromolecules* **2000**, *33* (16), 6126−6133.
(37) Schild, H. G.; Tirrell, D. A. *J. Phys. Chem.* **1990**, *94* (10), 4352−4356.
(38) Marchetti, M.; Prager, S.; Cussler, E. L. *Macromolecules* **1990**, *23* (6), 1760−1765.
(39) Fujishige, S.; Kubota, K.; Ando, I. *J. Phys. Chem.* **1989**, *93*, (8), 3311−3313.
(40) Flory, P. J.; Rehner, J. *J. Chem. Phys.* **1943**, *11* (11), 521−526.
(41) Flory, P. J. *J. Chem. Phys.* **1950**, *18* (1), 108−111.
(42) Suzuki, A.; Kojima, S. *J. Chem. Phys.* **1994**, *101* (11), 10003−10007.

MA071438N